RSC Advances

ROYAL SOCIETY OF CHEMISTRY

www.rsc.org/advances

Synthesis and characterization of novel electrochromic poly(amide-imide)s with *N,N'*-di(4-methoxyphenyl)-*N,N'*-diphenyl-*p*-phenylenediamine units†

Sheng-Huei Hsiao,*[a] Chia-Yin Teng,[a] Yu-Ruei Kung[b]

[a]*Department of Chemical Engineering and Biotechnology, National Taipei University of Technology, Taipei 10608, Taiwan. Correspondence to: S.-H. Hsiao (E-mail: shhsiao@ntut.edu.tw)*

[b]*Div. of Organic Opto-electronic Materials and Applications, Material and Chemical Laboratories, Industrial Technology Research Institute, Hsinchu 31040, Taiwan.*

†Electronic supplementary information (ESI) available. See DOI: 10.1039/xxx

(Abstract)

We developed a new efficient synthetic procedure for the synthesis of a bistriphenylamine diamine monomer, *N,N'*-bis(4-aminophenyl)-*N,N'*-bis(4-methoxyphenyl)-1,4-phenylenediamine (**3**). A new dicarboxylic acid monomer bearing two built-in imide rings, namely *N,N'*-bis(trimellitimidophenyl)-*N,N'*-bis(4-methoxyphenyl)-1,4-phenylenediamine (**4**), was synthesized from condensation of diamine **3** with two equivalent amount of trimellitic anhydride. Several novel electroactive poly(amide-imide)s (PAIs) containing *N,N'*-di(4-methoxyphenyl)-*N,N'*-diphenyl-*p*-phenylenediamine [TPPA(OMe)$_2$] units have been prepared by the phosphorylation polyamidation reactions from diamine **3** with four imide ring-preformed dicarboxylic acids or from diimide-diacid **4** with 4,4'-oxydianiline and diamine **3**, respectively. All the PAIs were readily soluble in many organic solvents and could be solution-cast into tough and flexible polymer films. These PAIs exhibited glass-transition temperatures (T_gs) in the range of 206-292 °C, and most of them did not show significant weight-loss before 450 °C. The PAI films revealed reversible electrochemical oxidation processes accompanied with strong color changes from the pale yellow neutral state to yellowish green and deep blue oxidized. Incorporating the TPPA(OMe)$_2$ unit on the amide side of PAIs led to lower oxidation potentials and higher redox and electrochromic stability.

1. Introduction

Electrochromism is defined as a reversible change in optical absorption (or transmittance) and color change resulting from the redox of the material in response to an externally applied potential by electrochemical means which has stimulated the interest of scientists over the past decades.[1] Traditionally, interest in electrochromic materials has been directed towards optical changes in the visible region, leading to many technological applications such as variable reflectance mirrors, smart windows, and electrochromic displays.[2-4] One of the main use of electrochromic materials is in smart windows for car and buildings[5] and in automatic-dimming rear-view mirrors.[6] Recent high-profile commercialization of electrochromic materials includes the Boeing 787 Dreamliner windows manufactured by Gentex.[7] Potential applications in information storage,[8] electrochromic displays,[9] and adaptive camouflages[10] can also be envisioned. There are several chemical systems that are

intrinsically electrochromic, such as transition metal oxides (especially tungsten oxide), inorganic coordination complexes, small organic molecules, and conjugated polymers (polyanilines, polypyrroles, and polythiophenes).[1-4] Electrochromic applications based on π-conjugated polymers become popular owing to their ease of colour-tuning, fast switching time, and high contrast ratios.[11-15] Studies from the Reynolds research group have shown a wide variety of conjugated polymers with colour changes that cover the entire visible spectrum.[16-20]

Triarylamine derivatives are well known for photo- and electroactive properties that find optoelectronic applications as photoconductors, hole-transporters, and light-emitters.[21-23] During the last decade, Liou's and our research groups have developed a number of high-performance polymers, such as aromatic polyamides and polyimides, carrying the triarylamine unit as an electrochromic functional moiety.[24-32] Our strategy was to synthesize the triarylamine-containing monomers such as diamines and dicarboxylic acids that were then reacted with the corresponding co-monomers through conventional polycondensation techniques. The obtained polymers possessed characteristically well-defined structures, high molecular weights, and high thermal stability. Because of the incorporation of packing-disruptive, propeller-shaped triarylamine units along the polymer backbone, almost all the polyamides and some of the polyimides exhibited good solubility in polar organic solvents. They could form uniform, transparent amorphous thin films by solution casting and spin-coating methods. This is advantageous for their ready fabrication of large-area, thin-film devices.

Aromatic poly(amide-imide)s (PAIs) possess balanced characteristics between polyamides and polyimides such as high thermal stability and good mechanical properties together with ease of processability.[33] Since we successfully applied the Yamazaki-Higashi phosphorylation reaction[34] to the direct synthesis of high-molecular-weight PAIs from the imide ring-preformed dicarboxylic acids and aromatic diamines using triphenyl phosphite (TPP) and pyridine as condensing agents, this efficient synthetic route has proved to exhibit significant advantages in preparing operations as compared with conventional acid chloride or isocyanate methods.[35] Thus, many novel PAIs have been readily prepared by this convenient technique in our and other laboratories.[36] Furthermore, this synthetic procedure can offer us the option of the incorporation of specific functionalities between amide or imide groups in the PAI backbone. The incorporation of such functional groups may provide a method of controlling certain physical properties or special functions of the resulting PAIs.

The anodic oxidation pathways of triphenylamine (TPA) derivatives were well studied.[37] The electrogenerated cation radical of TPA is not stable and could dimerize to form tetraphenylbenzidine by tail to tail coupling with loss of two protons per dimer. When the phenyl groups were incorporated by electron-donating substituents such as *tert*-butyl and methoxy groups at the *para*-position of TPA, the coupling reactions were greatly prevented by affording stable cationic radicals and lowering the oxidation potentials.[38] The redox property, electron-transfer process, and multi-colour electrochromic behaviour of the polymers bearing *N,N,N′,N*′-tetraphenyl-1,4-phenylenediamine (TPPA) segments are

interesting for electro-optical applications.[39-44] As reported by Yen and Liou in 2009, a methoxy-blocked TPPA-based diamine monomer *N,N'*-bis(4-aminophenyl)-*N,N'*-bis(4-methoxyphenyl)-1,4-phenylenediamine (Compound **3** as shown in Scheme 1) was synthesized and used for the preparation of highly organosoluble and stable visible/near-infrared electrochromic aromatic polyamides.[45] However, the polyimides based on diamine **3** were less soluble in organic solvents as compared to their polyamide counterparts.[46] Unless bridged dianhydrides such as ODPA, DSDA, and 6FDA were used, the polyimides derived from rigid diahnydrides such as PMDA were sparingly soluble in organic solvents. As a continuation of our efforts in developing easily processable high-performance functional polymers with the TPPA segment, the present study describes a new convenient and efficient synthetic route of the TPPA$(OMe)_2$-diamine **3** and the synthesis and characterization of its derived novel TPPA$(OMe)_2$-containing PAIs. The PAIs are expected to exhibit good solubility while preserve high thermal stability and good redox activity. The effects of the location of TPPA$(OMe)_2$ (i.e., on the imide side or the amide side) on the electrochemical and electrochromic properties of the PAIs are also investigated.

2. Experimental section

2.1. Materials

The diimide-diacid monomers **5a** and **5b** and monoimide-diacid **5c** and **5d** were prepared according to the previously reported procedures.[35] 4,4'-Oxydianiline (ODA) was used as received from Tokyo Chemical Industry (TCI). *N*-Methyl-2-pyrrolidone (NMP) (Tedia) was dried over calcium hydride for 24 h, distilled under reduced pressure, and stored over 4 Å molecular sieves in a sealed bottle. Triphenyl phosphite (TPP) (TCI) was used as received from the supplier. Commercially obtained calcium chloride ($CaCl_2$) was dried under vacuum at 180 ^{o}C for 3 h prior to use. Tetrabutylammonium perchlorate (Bu_4NClO_4) (TCI) was recrystallized twice from ethyl acetate under nitrogen atmosphere and then dried in *vacuo* prior to use. All other reagents and solvents were used as received from commercial sources.

2.2. Monomer synthesis

2.2.1. *N,N'*-Bis(4-methoxyphenyl)-1,4-phenylenediamine (1). Hydroquinone (22.02 g, 0.2 mol), *p*-anisidine (54.2 g, 0.44 mol), iodine (5.08 g, 0.04 mol), and 50 mL of xylene were placed in a 100-mL round-bottomed flask equipped with a short path distillation head. The mixture was heated to reflux for 20 h under nitrogen with removal of water. After that, the mixture was poured into 120 mL of ethanol, and the precipitated product was filtered and washed thoroughly with ethanol. Recrystallization from toluene afforded 34.3 g (57 % yield) of pale purple crystals with a melting point of 196−199 ^{o}C (by DSC at a heating rate of 10 ^{o}C min^{-1}). IR (KBr): 3386 cm^{-1} (N−H stretch). ^{1}H NMR (600 MHz, DMSO-d_6, δ, ppm): 3.68 (s, 6H, −OCH_3), 6.80 (s, J = 9.0 Hz, 4H, H_c), 6.88 (s, 4H, Ha), 6.91 (d, J = 9.0 Hz, 4H, H_b), 7.46 (s, 2H, N−H).

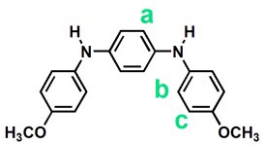

2.2.2. *N,N'*-Bis(4-methoxyphenyl)-*N,N'*-bis(4-nitrophenyl)-1,4-phenylenediamine (2). In a 250-mL round-bottom flask equipped with a stirring bar, a mixture of 9.6 g (0.03 mol) of *N,N'*-bis(4-methoxyphenyl)-1,4-phenylenediamine **(1)**, 9.3 g (0.066 mol) of *p*-fluoronitrobenzene, and 10.1 g of cesium fluoride (CsF) in 100 mL of dimethyl sulfoxide (DMSO) was heated at 150 °C for about 18 h. After cooling, the mixture was poured into 500 mL of methanol, and the precipitated product was collected by filtration. Recrystallization from DMF/methanol yielded 10.5 g (62%) of red crystals with a melting point of 228–232 °C (by DSC). IR (KBr): 1585, 1311 cm^{-1} ($–NO_2$ stretch). ^1H NMR (600 MHz, $CDCl_3$, δ, ppm): 3.84 (s, 6H, $–OCH_3$), 6.88 (d, J = 9.0 Hz, 4H, H_d), 6.95 (d, J = 9.0 Hz, 4H, H_c), 7.14 (s, 4H, H_a), 7.15 (d, J = 9.0 Hz, 4H, H_b), 8.03 (d, J = 9.0 Hz, 4H, H_e).

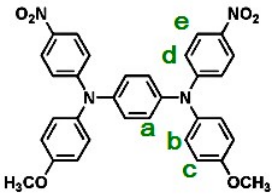

2.2.3. *N,N'*-Bis(4-aminophenyl)-*N,N'*-bis(4-methoxyphenyl)-1,4-phenylenediamine (3). In a 500 mL three-neck round-bottomed flask equipped with a stirring bar under nitrogen atmosphere, 2.32 g (4.12 mmol) of dinitro compound **2** and 0.1 g of 10% Pd/C were dispersed in 250 mL of ethanol. The suspension solution was heated to reflux, and 2 mL of hydrazine monohydrate was added slowly to the mixture. After a further 18 h of reflux, the solution was filtered to remove Pd/C, and the filtrate was cooled under nitrogen atmosphere. Yellowish green crystals grew during the cooling process of the filtrate. The precipitated crystals were collected by filtration and dried in vacuo at 80 °C to give 0.85 g (82% in yield) of pure diamino compound **3**; mp = 199–201 °C (by DSC). IR (KBr): 3450, 3365 cm^{-1} ($–NH_2$ stretch). ^1H NMR (600 MHz, DMSO-d_6, δ, ppm): 3.68 (s, 6H, $–OCH_3$), 4.92 (s, 4H, $–NH_2$), 6.53 (d, J = 8.4 Hz, 4H, H_e), 6.68 (s, 4H, H_a), 6.76 (d, J = 8.4 Hz, 4H, H_d), 6.80 (d, J = 9.0 Hz, 4H, H_c), 6.87 (d, J = 9.0 Hz, 4H, H_b). ^{13}C NMR (150 MHz, DMSO-d_6, δ, ppm): 55.1 ($–OCH_3$), 114.5 (C^5), 114.9 (C^9), 121.7 (C^1), 123.8 (C^4), 126.7 (C^8), 136.4 (C^7), 141.6 (C^3), 142.0 (C^2), 145.1 (C^{10}), 154.1 (C^6).

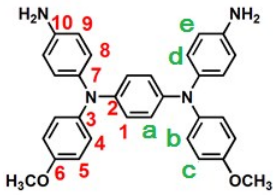

2.2.4. *N,N'*-Bis(trimellitimidophenyl)-*N,N'*-bis(4-methoxyphenyl)-1,4-phenylenediamine (4). A flask was charged with 1.92 g (10 mmol) of trimellitic anhydride, 2.51 g (5 mmol) of diamine **3**, and 60 mL of glacial acetic acid. The heterogeneous mixture was stirred for 1 h at room temperature and then refluxed at 120 °C for 12 h. Then, the mixture was poured into 200 mL of methanol, and the precipitate was collected by filtration and washed thoroughly with methanol to remove acetic acid.

The product was washed several times with hot water and then dried in vacuum to afford 3.49 g (82% yield) of the diimide-diacid monomer **4** as red-brown powder; mp = 332−336 °C. The product could be directly used for the subsequent polymerization reaction without any further purification. IR (KBr): 2700−3500 cm^{-1} (carboxyl O−H stretch), 1776, 1725 cm^{-1} (imide and carboxyl C=O stretch). ^{1}H NMR (600 MHz, DMSO-d_6, δ, ppm): 13.57 (a broad hump, 2H, –COOH), 3.76 (s, 6H,−OCH_3), 6.96−6.98 (two overlapped doublets, 8H, H_{c+d}), 7.05 (s, 4H, H_a), 7.14 (d, J = 9.0 Hz, 4H, H_b), 7.27 (d, J = 9.0 Hz, 4H, H_e), 8.05 (d, J = 7.8 Hz, 2H, H_f), 8.28 (d, J = 1.2 Hz, 2H, H_h), 8.39 (dd, J = 7.8, 1.2 Hz, 2H, H_g).

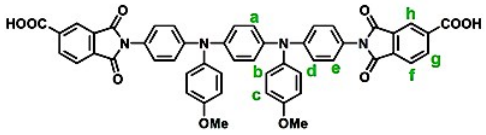

2.3. Synthesis of PAIs

The synthesis of PAI **7a** was used as an example to illustrate the general synthetic route to produce the PAIs. A mixture of 0.5105 g (0.6 mmol) of diimide-diacid monomer **4**, 0.1201 g (0.6 mmol) of ODA , 0.1 g of anhydrous calcium chloride, 0.6 mL of triphenyl phosphite (TPP), 0.15 mL of pyridine, and 0.6 mL of NMP was heated with stirring at 120 °C for 3 h. The resulting polymer solution was poured slowly into 150 mL of methanol giving rise to a tough, fibrous precipitate. The precipitated product was collected by filtration, washed thoroughly with hot water and methanol, and then dried to give PAI **7a**. The inherent viscosity of the polymer was 0.76 dL/g, measured in DMAc at a concentration of 0.5 g/dL at 30 °C. The IR spectrum of **7a** (film) exhibited characteristic amide absorption bands at 3280 cm^{-1} (amide N−H stretch) and 1668 cm^{-1} (amide carbonyl stretch), together with the imide absorption bands at 1778 cm^{-1} (asymmetrical C=O stretch) and 1720 cm^{-1} (symmetrical C=O stretch).

2.4. Preparation of the PAI films

A solution of the polymer was made by dissolving about 0.6 g of the PAI sample in 9 mL of hot DMAc. The homogeneous solution was poured into a 7-cm glass Petri dish, which was placed in a 90 °C oven overnight for the slow release of the solvent. The cast film was then released from the glass substrate and was further dried in vacuo at 160 °C for 8 h. The obtained films were about 75 μm in thickness and were used for thermal analyses.

2.5. Instrumentation and measurements

Infrared (IR) spectra were recorded on a Horiba FT-720 FT-IR spectrometer. ^{1}H and ^{13}C NMR spectra were measured on a Bruker Avance III HD-600 MHz NMR spectrometer with tetramethylsilane as an internal standard. The inherent viscosities were determined with a Cannon-Fenske viscometer at 30 °C. Thermogravimetric analysis (TGA) was performed with a Perkin-Elmer Pyris 1 TGA instrument. Experiments were carried out on approximately 4−6 mg of film samples heated in flowing nitrogen or air (flow rate = 40 cm^3 min^{-1}) at a heating rate of 20 °C min^{-1}. DSC analyses were performed on a

Perkin-Elmer DSC 4000 differential scanning calorimeter at a scan rate of 20 ^{o}C min^{-1} in flowing nitrogen. Electrochemistry was performed with a CHI 750A electrochemical analyzer. Cyclic voltammetry was conducted with the use of a three-electrode cell in which ITO (polymer film area about 0.8 cm x 1.25 cm) was used as a working electrode. A platinum wire was used as an auxiliary electrode. All cell potentials were taken with the use of a home-made Ag/AgCl, KCl (sat.) reference electrode. Ferrocene was used as an external reference for calibration (+0.48 V vs Ag/AgCl). Voltammograms are presented with the positive potential pointing to the left and with increasing anodic currents pointing downwards. Spectroelectrochemistry analyses were carried out with an electrolytic cell, which was composed of a 1 cm cuvette, ITO as a working electrode, a platinum wire as an auxiliary electrode, and a Ag/AgCl reference electrode. Absorption spectra in the spectroelectrochemical experiments were measured with an Agilent 8453 UV-Visible diode array spectrophotometer.

3. Results and discussion

3.1. Monomer synthesis

The TPPA(OMe)$_2$-diamine monomer **3** was synthesized by a three-step reaction sequence as shown in Scheme 1. In the first step, *N,N*'-bis(4-methoxyphenyl)-1,4-phenylenediamine (**1**) was synthesized by condensation of hydroquinone with *p*-anisidine in the presence of small amounts of iodine according to the Knoevenagel synthesis of aromatic secondary amines.[47] In the second step, the intermediate dinitro compound, *N,N*'-bis(4-methoxyphenyl)-*N,N*'-bis(4-nitrophenyl)-1,4-phenylenediamine (**2**) was obtained by the nucleophilic aromatic fluoro-displacement reaction of *p*-fluornitrobenzene with the secondary amine **1** in the presence of cesium fluoride (CsF). Finally, the target diamine monomer **3** was prepared by hydrazine Pd/C-catalyzed reduction of dinitro compound **2**. The yield of crude product in each step was generally higher than 80%. This strategy for the preparation of diamine **3** seems to be more convenient and more efficient than that using Ullmann reaction reported by Yen and Liou.[45]

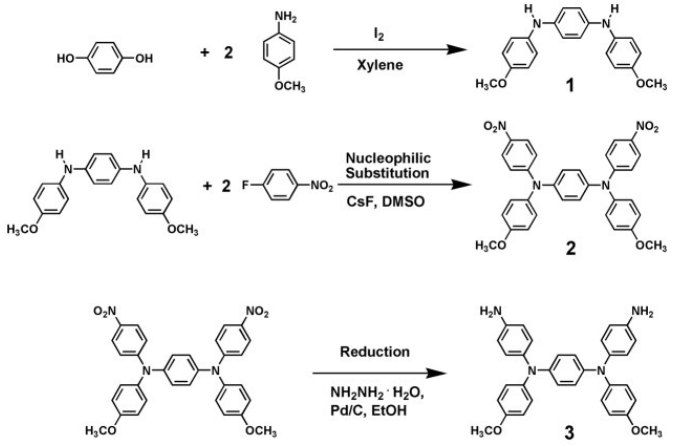

Scheme 1 Synthetic route to the TPPA(OMe)$_2$-diamine monomer **3**.

Fig. S1 (Supplementary Information; SI) illustrates FT-IR spectra of compounds **1** to **3**. The IR spectrum of compound **1** gives rise to a sharp, medium absorption at about 3386 cm^{-1} ascribed to the secondary amine N−H stretching vibration. The dinitro compound **2** shows the characteristic absorption of nitro groups at around 1585 and 1311 cm^{-1} (−NO_2 asymmetric and symmetric stretching). After reduction, the characteristic absorptions of the nitro group disappeared and the amino group shows the typical −NH_2 stretching absorption pair at 3450 and 3365 cm^{-1} as shown in the IR spectrum of diamine **3**. The ^{1}H NMR spectrum of the secondary amine **1** is illustrated in Fig. S2 (SI). The aromatic NH groups appear at 7.46 ppm as a sharp singlet, and the tall singlet at 3.68 ppm is attributed to the methoxy groups. The hydrogens on the benzene rings appear in the range of 6.79−6.93 ppm. The ^{1}H and H-H COSY NMR spectra of the dinitro monomer **2** are compiled in Fig. S3 (SI). The ^{1}H, H-H COSY, ^{13}C and C-H HMQC NMR spectra of the diamine monomer **3** are compiled in Figs. 1 and 2, respectively. These ^{1}H and ^{13}C NMR spectra are essentially identical to those reported in literature,[50] where the intermediate dinitro compound **2** has been prepared by a different synthetic route. Only a slight difference in chemical shifts of the resonance peaks was observed possibly due to the use of different test solvents. The ^{1}H NMR spectra confirm that the nitro groups have been completely transformed into amino groups by the high field shift of the aromatic protons, especially for protons H_e *ortho* to the amino group, and the resonance signal at about 4.92 ppm corresponding to the aryl primary amino protons. The assignments of all hydrogen and carbon atoms are assisted by two-dimensional (2-D) NMR spectra and are consistent with the proposed structures of compounds **2** and **3**.

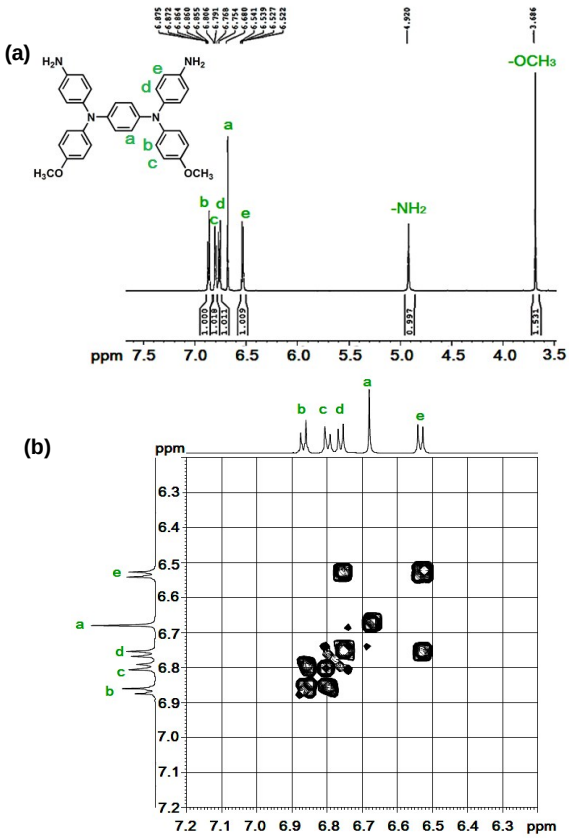

Fig. 1 (a) ^{1}H and (b) H-H COSY NMR spectra of diamine **3** in DMSO-d_6.

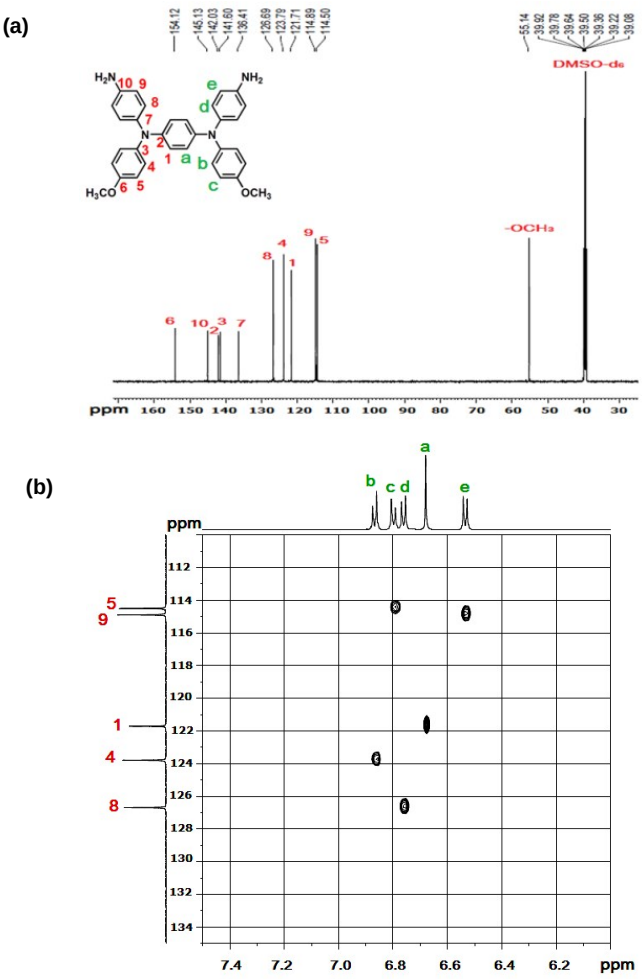

Fig. 2 (a) ^{13}C and (b) C-H HMQC NMR spectra of diamine **3** in DMSO-d_6.

The new diimide-diacid monomer **4** containing the TPPA(OMe)$_2$ unit was synthesized by condensation of diamine **3** with two molar equivalent amount of trimellitic anhydride (TMA) in refluxing glacial acetic acid (Scheme 2). The structure of diimide-diacid **4** was confirmed by IR and ^{1}H NMR spectroscopies. As shown in Fig. S4 (SI), the IR spectrum of diimide-diacid **4** shows absorption bands around 2700-3500 cm^{-1} (–OH stretch, carboxylic acid), 1776 (imide C=O asymmetrical stretching), and 1725 cm^{-1} (imide C=O symmetrical stretching and carboxyl C=O stretching), confirming the presence of imide ring and carboxylic acid groups in the structure. Fig. 3(a) shows the high-resolution ^{1}H NMR spectrum of **4** in deuterated dimethyl sulfoxide (DMSO-d_6). Assignments of each proton are assisted by the H-H COSY NMR spectrum (Fig. 3(b)), and the spectra agree well with the proposed molecular structure of **4**.

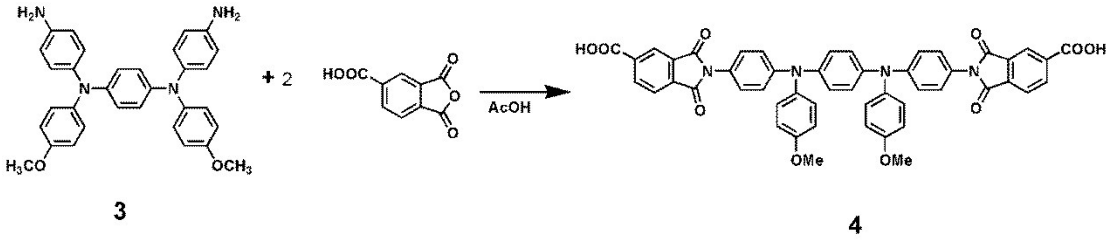

Scheme 2 Synthesis of diimide-diacid monomer **4**.

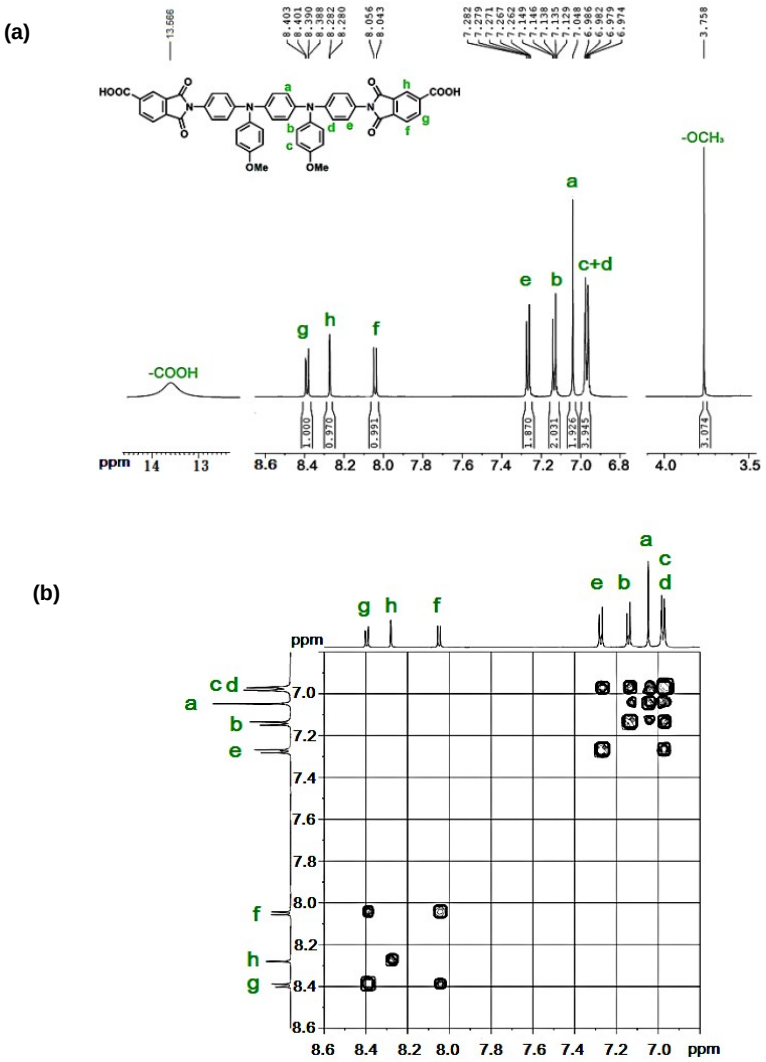

Fig. 3 (a) ^{1}H and (b) H-H COSY NMR spectra of diimide-diacid monomer **4** in DMSO-d_6.

3.2. Synthesis of PAIs

According to the phosphorylation polyamidation technique described by Yamazaki and co-workers,[34] a series of novel PAIs **6a–6d** were synthesized from various combinations of diamine **3** with imide ring-preformed dicarboxylic acids shown in Scheme 3 by using triphenyl phosphite (TPP) and pyridine (Py) as condensing agents. Another type of PAIs **7a** and **7b** were prepared from ODA and diamine **3**, respectively, with the newly synthesized diimide-diacid **4** by a similar synthetic technique (Scheme 4).

All the polymerization reactions proceeded homogeneously throughout the reaction and afforded clear, highly viscous polymer solutions. All the polymers precipitated in a tough, fiber-like form when the resulting polymer solutions were slowly poured under stirring into methanol. The obtained PAIs had inherent viscosities in the range of 0.72-0.84 dL g^{-1}, as listed in Table 1. All the polymers can be solution-cast into flexible and transparent films, indicating the formation of high molecular weight polymers.

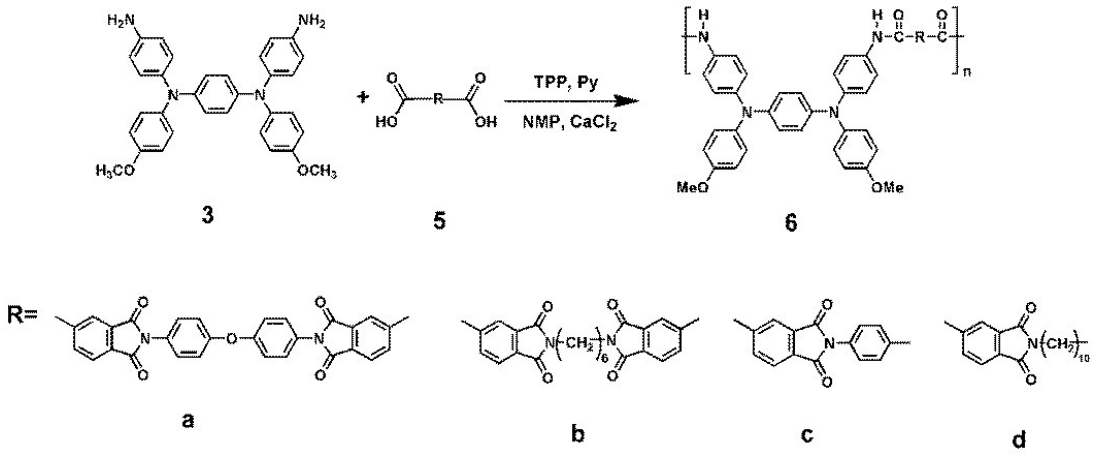

Scheme 3 Synthesis of PAIs **6a–6d**.

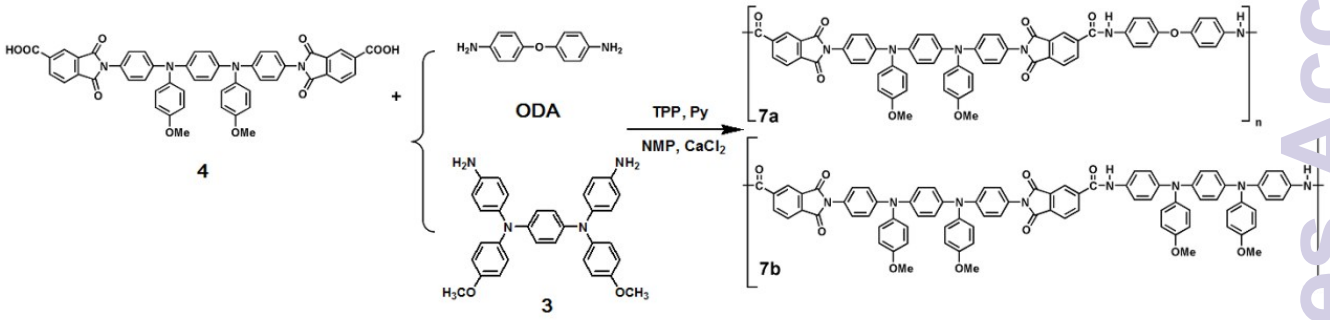

Scheme 4 Synthesis of PAIs **7a** and **7b**.

The structures of the PAIs were confirmed by IR and NMR spectroscopy. Fig. S5 (SI) shows the IR spectra of PAIs **6a–6d**, and Fig. S6 illustrates those of PAIs **7a** and **7b**. All the PAIs showed the characteristic absorption bands of the amide group at around 3288 cm^{-1} (N–H stretching) and 1668 cm^{-1} (amide C=O) , and the characteristic imide absorption bands at around 1774 cm^{-1} (asymmetric C=O) and 1722 cm^{-1} (symmetric C=O). As a representative example, the ^{1}H and H-H COSY NMR spectra of PAI **7a** are compiled in Fig. 4. The proton NMR spectra of another two examples for PAIs **6a** and **7b** are respectively depicted in Figs. S7 and S8 (SI). The specific assignment of individual hydrogen atoms could be made with the aid of 2-D NMR spectra. All the spectra agree well with the proposed repeating units in these PAIs.

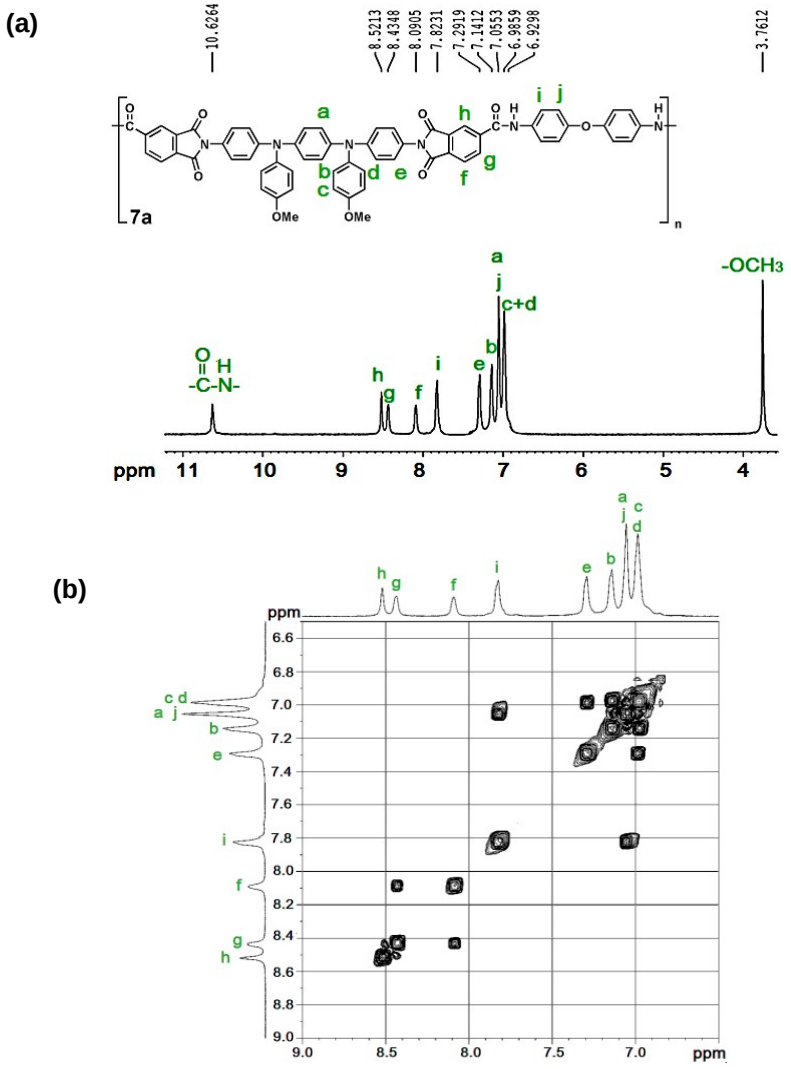

Fig. 4 (a) ^{1}H and (b) H-H COSY NMR spectra of PAI **7a** in DMSO-d_6.

3.3. Properties of PAIs

3.3.1. Solubility

The qualitative solubility properties of PAIs in several organic solvents at 10% (w/v) are summarized in Table 1. All of the PAIs were readily dissolved in polar aprotic solvents such as NMP, DMAc, and DMF at room temperature. They are also easily soluble in m-cresol. However, most of them are sparingly soluble in DMSO and less polar THF. The high solubility of these PAIs can be attributed to the incorporation of bulky, packing-disruptive, and three-dimensional TPPA(OMe)2 units in the polymer structure, which results in a high steric hindrance for close packing and thus reduces their crystallization tendency and interchain interactions. Therefore, the good solubility to most polar organic solvents makes these polymers potential candidates for practical applications by simple solution processing.

Table 1 Inherent viscosity and solubility behavior of PAIs

Polymer code	η_{inh} (dL/g)[a]	Solubility in various solvents[b, c]					
		NMP	DMAc	DMF	DMSO	*m*-Cresol	THF
6a	0.84	++	++	++	++	++	−−
6b	0.79	++	++	++	+−	++	+−
6c	0.75	++	++	++	+−	++	−−
6d	0.80	++	++	++	++	++	+−
7a	0.76	++	++	++	++	++	+−
7b	0.72	++	++	++	+−	++	−−

[a] Inherent viscosity measured at a concentration of 0.5 dL/g in DMAc at 30 °C. [b] Solvent: NMP: *N*-methyl-2-pyrrolidone; DMAc: *N,N*-dimethylacetamide; DMF: *N,N*-dimethylformamide; DMSO: dimethyl sulfoxide; THF: tetrahydrofuran. [c] The qualitative solubility was tested with 10 mg of a sample in 1 mL of stirred solvent. ++, soluble at room temperature; +−, partially soluble on heating; −−, insoluble even on heating.

3.3.2. Thermal properties

The thermal properties of all the PAIs were investigated by DSC and TGA techniques. The thermal behavior data of PAIs are summarized in Table 2. Typical TGA and DSC curves of the representative PAI **7b** are shown in Fig. 5. The glass-transition temperatures (T_g) of these PAIs could be easily determined by the DSC method; they were observed in the range of 206−292 °C (see Fig. S9 in SI**)**. Semi-aromatic PAIs **6b** and **6d** exhibited relatively lower T_g values (218 and 206 °C, respectively) when compared with wholly aromatic PAIs **6a** (T_g = 287 °C) and **6c** (T_g = 278 °C) due to the presence of flexible polymethylene segments. PAIs **7a** (T_g = 285 °C) and **7b** (T_g = 292 °C) also reveal high T_gs because of high aromatic content. All of the aromatic PAIs exhibited a similar TGA pattern with no significant weight loss below 450 °C in air or nitrogen atmosphere. The decomposition temperatures (T_d) at which a 10% weight-loss of the PAIs in nitrogen and air were recorded in the range of 474−548 °C and 457−540 °C, respectively. As expected, PAIs **6b** and **6d** decompose at slightly lower temperatures than other PAIs because of the less stable aliphatic segments. The amount of carbonized residue (char yield) of all the PAIs in nitrogen atmosphere was more than 58% at 800 °C. The high char yields of the aromatic PAIs can be ascribed to their high aromatic content. The thermal analysis results revealed that these PAIs generally exhibited good thermal stability, which in turn is beneficial to increase the service time in device application and enhance the morphological stability to the spin-coated films.

Table 2 Thermal properties of PAIs

Polymer code[a]	T_g (°C)[b]	T_d at 5% weight loss (°C)[c]		T_d at 10% weight loss (°C)[c]		Char yield (wt%)[d]
		N_2	Air	N_2	Air	
6a	287	496	488	548	540	68
6b	218	482	465	502	497	63
6c	278	480	465	515	509	67
6d	206	443	414	474	457	58
7a	285	487	491	530	535	69
7b	292	496	483	548	539	71

[a] All the polymer film samples were heated at 300 °C for 1 h before all the thermal analyses. [b] Midpoint temperature of the baseline shift on the second DSC heating trace (rate = 20 °C min^{-1}) of the sample after quenching from 400 to 50 °C (rate = 20 °C min^{-1}) in nitrogen. [c] Decomposition temperature at which a 5% or 10% weight loss was recorded by TGA at a heating rate of 20 °C min^{-1} and a gas flow rate of 20 cm^3 min^{-1}. [d] Residual weight % at 800 °C at a scan rate 20 °C min^{-1} in nitrogen.

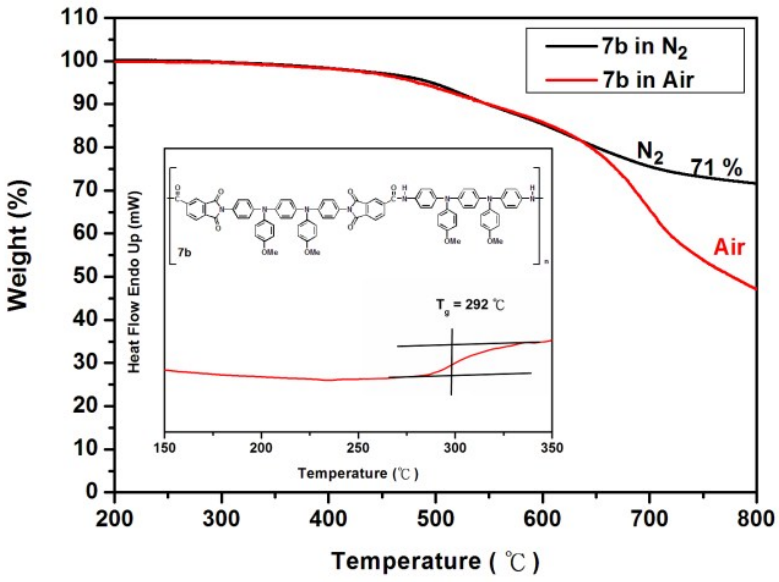

Fig. 5 TGA and DSC curves of PAI **7b** with a heating rate 20 °C min^{-1}.

3.3.3. Electrochemical properties

The electrochemical behavior of the PAIs was investigated by cyclic voltammetry (CV) conducted for the cast films on an ITO-coated glass substrate as working electrode in dry acetonitrile (CH_3CN) (for anodic oxidation) containing 0.1 M of Bu_4NClO_4 as the supporting electrolyte using saturated Ag/AgCl as the reference electrode. The derived oxidation potentials are summarized in Table 3. All the **6** series PAIs exhibit two reversible oxidation redox couples with half-wave potentials ($E_{1/2)}$ in the ranges of 0.60−0.65 V and 0.95−1.00 V, respectively, corresponding to successive one electron removal from the $TPPA(OMe)_2$ units. The CV diagrams of PAI **6d**, representative for the other **6** series PAIs, are shown in Fig. 6. PAI **6d** exhibits very high electrochemical stability because of the active sites of the TPPA are blocked with methoxy groups. It displays two reversible oxidation processes with oxidation peaks at about 0.60 and 0.95 V, respectively. During the electrochemical oxidation of the PAI films, it was also found that the color of the film changed from pale yellow to yellowish green and then to dark blue. Because of the electrochemistry stability and good adhesion between the polymer thin film and the ITO substrate, **6d** still exhibited very high electroactivity after 100 repetitive cyclic scans between 0.0 V to 1.2 V.

The first anodic CV scans of PAIs **6a** and **7a** with an isomeric repeat unit are compared in Fig. 7. PAI **6a** revealed a lower oxidation potential (E_{onset} = 0.41 V, E_{pa} = 0.65 V) as compared to its isomeric PAI **7a** (E_{onset} = 0.49 V, E_{pa} = 0.74 V) because its $TPPA(OMe)_2$ unit is located in the amide side, which should be more easily oxidized than that in the imide side. PAI **7b** contains the $TPPA(OMe)_2$ segment in both amide and imide sides and is expected to show more oxidation processes. However, as shown in Fig. 8, PAI **7b** only showed two redox couples similar to other PAIs. The peaks are broader than those of other PAIs due to close overlapping of the redox waves..

The redox potentials of the PAIs as well as their respective highest occupied molecular orbital (HOMO) and lowest unoccupied molecular orbital (LUMO) (versus vacuum) energy levels are summarized in Table 3. The external ferrocene/ferrocenium (Fc/Fc^+) redox standard has $E_{1/2}$ value of 0.44 V vs Ag/AgCl in acetonitrile. Under the assumption that the HOMO level or called ionization potentials (versus vacuum) for the ferrocene standard was 4.80 eV with respect to the zero vacuum level, the HOMO levels for the PAIs are estimated from the $E_{1/2}^{Ox1}$ values of from their CV diagrams as 4.84−4.99 eV. The energy gaps estimated from the absorption spectra were then used to obtain the LUMO energy levels of 1.86−2.06 eV. The low ionization potentials suggest an easier hole injection into films from ITO electrodes in electronic device applications.

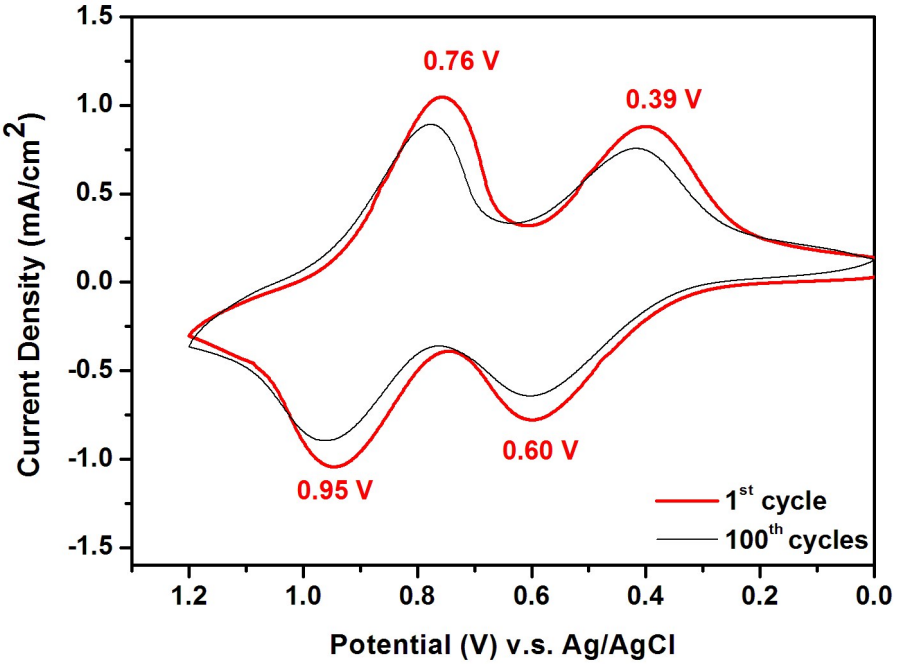

Fig. 6 Cyclic voltammograms of the cast film of PAI **6d** on the ITO-coated glass substrate in 0.1 M Bu_4NClO_4/CH_3CN at a scan rate of 50 mV s^{-1}.

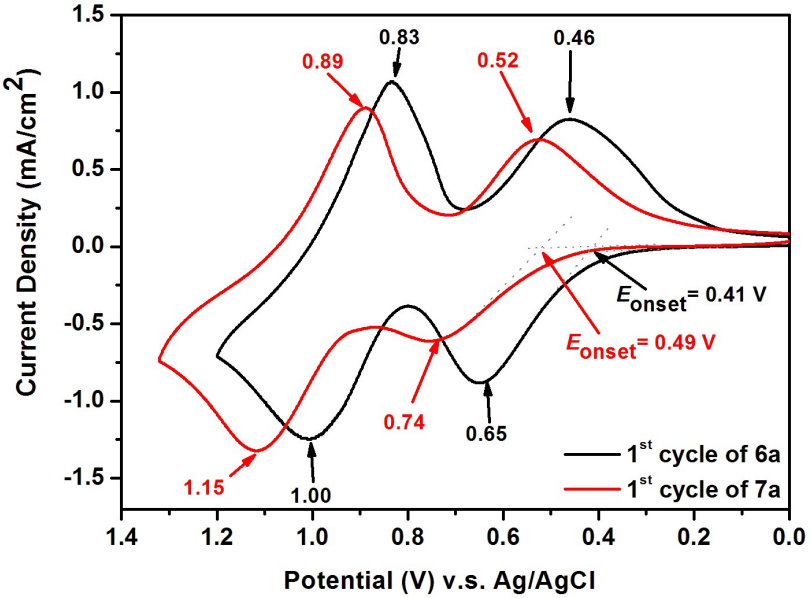

Fig. 7 Cyclic voltammograms of the cast films of PAIs **6a** and **7a** on the ITO-coated glass substrate in 0.1 M Bu_4NClO_4/CH_3CN at a scan rate of 50 mV s^{-1}.

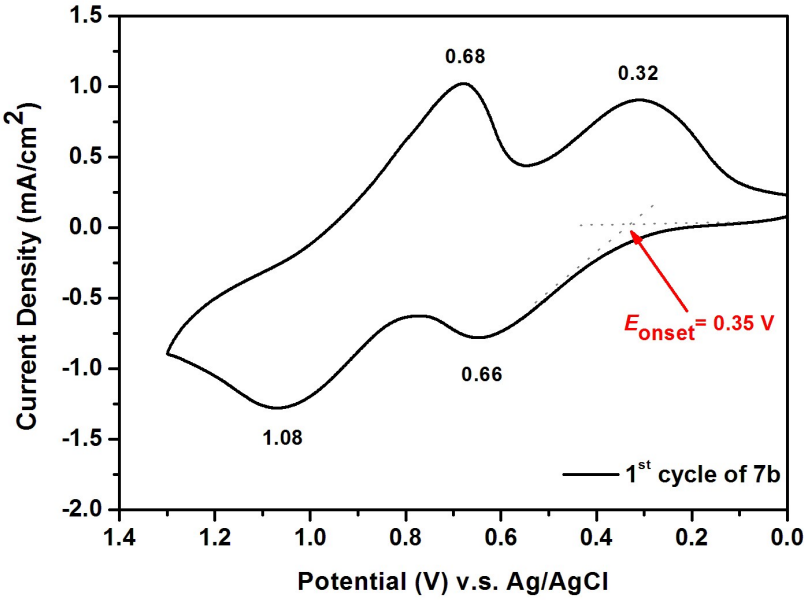

Fig. 8. Cyclic voltammogram of the cast film of **7b** on the ITO-coated glass substrate in 0.1 M Bu_4NClO_4/CH_3CN at a scan rate of 50 mV s^{-1}.

Table 3 Optical and electrochemical properties of PAIs

Polymer	UV-vis absorption (nm)[a]		Oxidation potential (V)[b]			Optical bandgap E_g (eV)[c]	HOMO (eV)[d]	LUMO (eV)[d]
	λ_{max}	λ_{onset}	E_{onset}	$E_{1/2}^{Ox1}$	$E_{1/2}^{Ox2}$			
6a	311	434	0.41	0.56	0.92	2.86	4.92	2.06
6b	310	426	0.38	0.51	0.87	2.91	4.87	1.96
6c	307	421	0.34	0.48	0.84	2.94	4.84	1.90
6d	320	413	0.35	0.50	0.86	3.00	4.86	1.86
7a	345	433	0.49	0.63	1.02	2.86	4.99	2.13
7b	315	422	0.35	0.49	0.88	2.94	4.85	1.91

[a] UV-vis absorption maximum and onset for the polymer films. [b] Calculated from first CV scans, versus Ag/AgCl in acetonitrile at a scan rate of 50 mV s^{-1}. [c] Optical bandgap calculated from absorption edge of the polymer film: $E_g = 1240/\lambda_{onset}$. [d] The HOMO energy levels were calculated from $E_{1/2}^{Ox1}$ values from the CV curves and were referenced to ferrocene (4.8 eV relative to the vacuum energy level, $E_{1/2}^{Ox} = 0.44$ V vs. Ag/AgCl). $E_{HOMO} = E_{1/2}^{Ox1} + 4.8 - 0.44$ (eV); $E_{LUMO} = E_{HOMO} - E_g$.

3.3.4. Spectroelectrochemical and electrochromic properties

Spectroelectrochemical measurements were performed on films of polymers drop-coated onto ITO-coated glass slides immerged in an electrolyte solution. The electrode preparations and solution conditions were identical to those used in the CV experiments. During the test, a three-electrode configuration was used for applying potential to the polymer films in a 0.1 M Bu_4NClO_4/CH_3CN electrolyte solution. When the films were electrochemically oxidized, a strong color change was observed.

Fig. 9(a) shows the spectral changes of PAI **6a** film upon oxidative scans from 0 to 1.00 V. In the neutral form, PAI **6a** exhibited strong absorption at λ_{max} of 311 nm due to the π-π* transitions. As the applied voltage was stepped from 0.0 to 0.65 V, the absorbance at 311 nm decreased, and new peak at 426 nm and a broadband from 985 nm extended into the near-infrared (NIR) region grew up. In the same time, the film turned into yellowish green. We attribute these spectral changes to the formation of a stable monocation radical in the $TPPA(OMe)_2$ moiety. The absorption band in the NIR region is assigned to an intervalence charge-transfer (IV-CT) between states in which the positive charge is centered at different amino centers.[48,49] As the applied voltage was raised to 1.00 V, the absorbance at 426 nm decreased and a new broad absorption band at 815 nm started to intensify. Meanwhile, the film changed color from yellowish green to dark blue as shown in the inset of Fig. 9(a). The spectral change of semi-aromatic PAI **6d** upon oxidation is very similar to that of **6a** (see Fig. S10 in SI). For comparison, the spectral change of the cast film of the isomeric PAI **7a** on ITO-glass upon oxidative scans is illustrated in Fig. 9(b). In the neutral form, the **7a** exhibited strong absorption at λ_{max} of 345 nm. As the applied voltage was stepped from 0.0 to 0.74 V, the absorbance at 345 nm decreased, and new peak at 425 nm and a broadband having its maximum around 980 nm in the NIR region grew up because of the IV-CT effect. In the same time, the film turned from nearly colorless into pale yellow due to the first oxidation process. At a higher applied potential of 1.15 V, the absorbance at 425 nm decreased and a new broad absorption band at 796 nm, a slight blue shift compared with that of isomeric **6a** (815 nm), started to intensify, and the film changed color from pale yellow to deep blue (see the inset shown in Fig. 9(b)).

A similar spectral change was observed for PAI **7b** at early stage of oxidation (Fig. 10). The absorption peak at 423 nm and the IV-CT band at 988 nm grew up when the applied potential was increased to 0.76 V. This result illustrates that the first two oxidations of the $TPPA(OMe)_2$ unit in both the amide and imide sides occurred almost simultaneously. Further increase of the applied potential over 0.95 V led to the increase of the absorption intensity at about 585 and 801 nm. This absorption change may be explained by the occurrence of the third oxidation. Upon further increase of the potential to 1.12 V, the intensity of the absorption band at 423 nm decreased and the bands around 585 and 801 nm further intensified. It was also found the IV-CT band in the NIR region diminished gradually, implying the occurrence of the fourth oxidation. When the polymer film of **7b** was electrochemically oxidized, its color changed from pale yellow to yellowish green, cyan, and deep blue, as can be seen from the inset of Fig. 10.

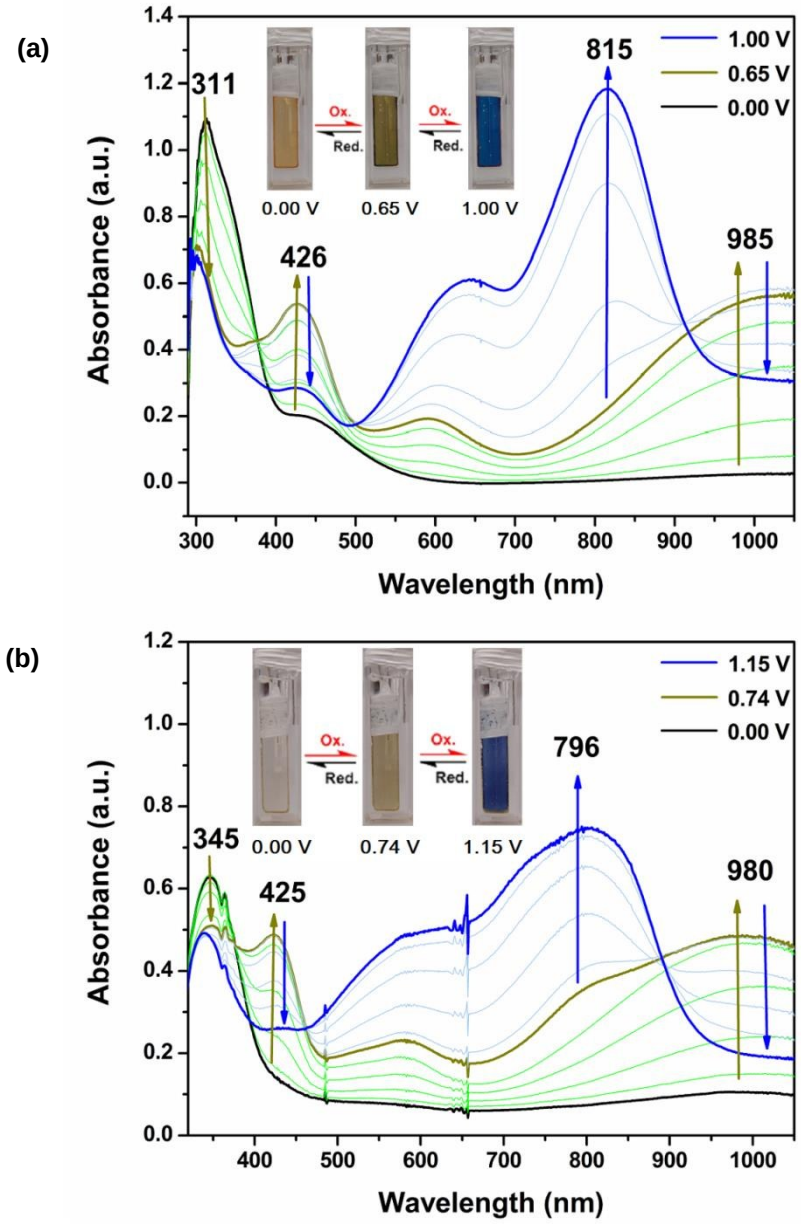

Fig. 9 Spectroelectrograms and color changes of (a) PAI **6a** (330 ± 50 nm in thickness) and (b) PAI **7a** (250 ± 20 nm in thickness) thin films on the ITO-coated glass substrate in 0.1 M Bu_4NClO_4/CH_3CN at various applied voltages (Inset: polymer films with about 1.6 μm in thickness).

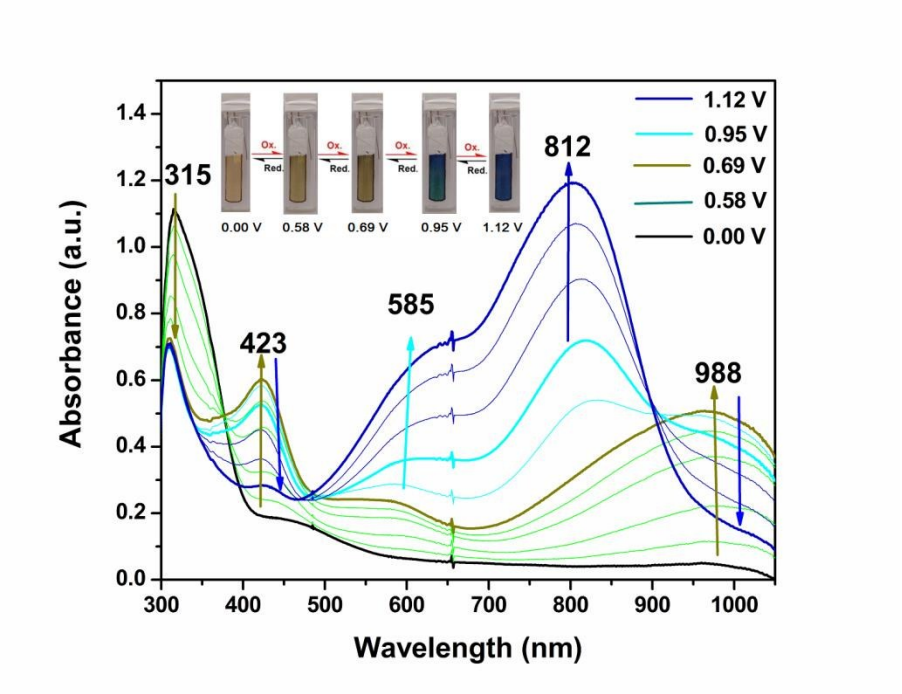

Fig. 10 Spectroelectrograms and color changes of PAI **7b** thin film (320 ± 30 nm in thickness) on the ITO-coated glass substrate in 0.1 M Bu_4NClO_4/CH_3CN (Inset: polymer film with 1.7 μm in thickness).

3.3.5. Electrochromic switching and stability

The stability, response time, and color efficiency are the key parameters for an electroactive polymer film to be amenable for usage in optical and electrochromic devices, thus the electrochromic switching studies were further measured. Electrochromic switching studies for the PAIs were performed to monitor the percent transmittance changes (ΔT%) as a function of time at their absorption maximum (λmax) and to determine the response time by stepping potential repeatedly between the neutral and oxidized states. The polymer film was cast onto an ITO-coated glass slides in the same manner as described earlier, and the active area of the polymer film on ITO glass is about 1 cm^2. When the films were switched, the absorbance at the given wavelength was monitored as a function of time with UV-vis-NIR spectroscopy. Figs. 11 and 12 depict the optical transmittance of **6a** film as a function of time at 426 and 815 nm by applying square-wave potential steps between 0 and 0.65 V and between 0 and 1.00 V for a switching time of 15 s. Generally, the charge passed at 90% of the full optical switch was used to evaluate the response time since the naked eye could not distinguish the color change after this point. As shown in Fig. 11(a), the polymer film of **6a** still exhibited very good electrochromic response after over 20 cyclic scans between 0 and 0.65 V. PAI **6a** film attained 90% of a complete coloring and bleaching in 4.8 and 2.1 s, respectively. The optical contrast measured as ΔT% between neutral pale yellow and oxidized yellowish green states was found to be 33 % at 426 nm [Fig. 11(b)]. When **6a** was switched between neutral and fully oxidized states (the applied potential switched between 0 and 1.00 V), almost no optical contrast loss was observed

during switching in the first twenty cycles [Fig. 12(a)]. The response times for coloring and bleaching are recorded as 3.6 and 4.1 s, respectively. The optical contrast between neutral pale yellow and oxidized deep blue states was found to be 73 % at 815 nm [Fig. 12(b)]. In addition, the electrochromic coloration efficiency (CE; η) can be calculated via optical density using the following equation:[1,2] $\eta = \Delta OD/Q_d$, where ΔOD is the optical absorbance change, and Qd (mC cm^{-2}) is the inject/ejected charge during a redox step. On the basis of this equation, the CE values of the **6a** film estimated from the data were found to be 318 cm^2 C^{-1} at 426 nm and 375 cm^2 C^{-1} at 815 nm.

The potential step absorptionmetry of the **6d** film is included in the Supplementary Information. Figs. S11 and S12 depict the optical transmittance of **6d** film as a function of time at 430 and 817 nm by applying square-wave potential steps between 0.00 and 0.70 V for a residence time of 7 s and between 0.00 and 1.05 V for a residence time of 12 s. As shown in Fig. S11(a), the polymer film of **6d** still exhibited very good electrochromic response after over 50 cyclic scans between 0 and 0.70 V. PAI **6d** film attained 90% of a complete coloring and bleaching in 2.2 and 1.4 s, respectively. The optical contrast measured as ΔT% between neutral pale yellow and oxidized yellowish green states was found to be 36 % at 430 nm [Fig. S11(b)]. When 6d was switched between neutral and fully oxidized states (the applied potential switched between 0 and 1.05 V), only a very small optical contrast loss was observed during switching [Fig. S12(a)]. The response times for coloring and bleaching are similar to those switching between neutral and first oxidized state. The optical contrast measured as ΔT% between neutral pale yellow and oxidized deep blue states was found to be 71 % at 817 nm [Fig. S12(b)].

The stability and switching behavior of the **7a** film at λ_{max} = 425 nm and 796 nm were investigated by monitoring the electrochromic contrast (ΔT%) of the thin film upon repeated square-wave potential steps between 0 and 0.75 V and between 0 and 1.15 V for a pulse width of 15 s. The results are shown in Figs. 13 and 14, respectively. In this case, a response time required for 90 % full-transmittance change of 3.9 s for the yellowish green coloring step and 2.2 s for the bleaching step at 425 nm and 3.5 s for the blue coloring step and 2.4 s for the bleaching step at 796 nm. In addition, the optical contrast measured (ΔT%) recorded at neutral and oxidized forms was found to be 32 % at 425 nm and 65 % at 796 nm. The CE values of the **7a** film were calculated as 284 cm^2 C^{-1} at 425 nm and 319 cm^2 C^{-1} at 796 nm (Table 4) by chronoamperometry. The **7a** film showed a larger loss of electrochromic contrast as compared to the **6a** film with the isomeric repeat unit in the first 20 scans. The less stability of the **7a** film might be attributable to the strong electron-withdrawing effect of the imide group. In contrast, the **6a** film exhibited excellent electrochromic stability because the $TPPA(OMe)_2$ unit is located in the amide side. The switching results of PAI **7b** are included in the Supporting Information. As shown in Fig. S13, PAI **7b** exhibits good stability in the first 20 full switches, and almost no optical contrast loss after 20 full switches was observed if the polymer film was switched between 0 and 1.15 V (Fig. S14). This result also indicated that incorporating the $TPPA(OMe)_2$ unit on the amide side of PAIs led to lower oxidation potentials, higher redox reversibility, and better electrohromic performance.

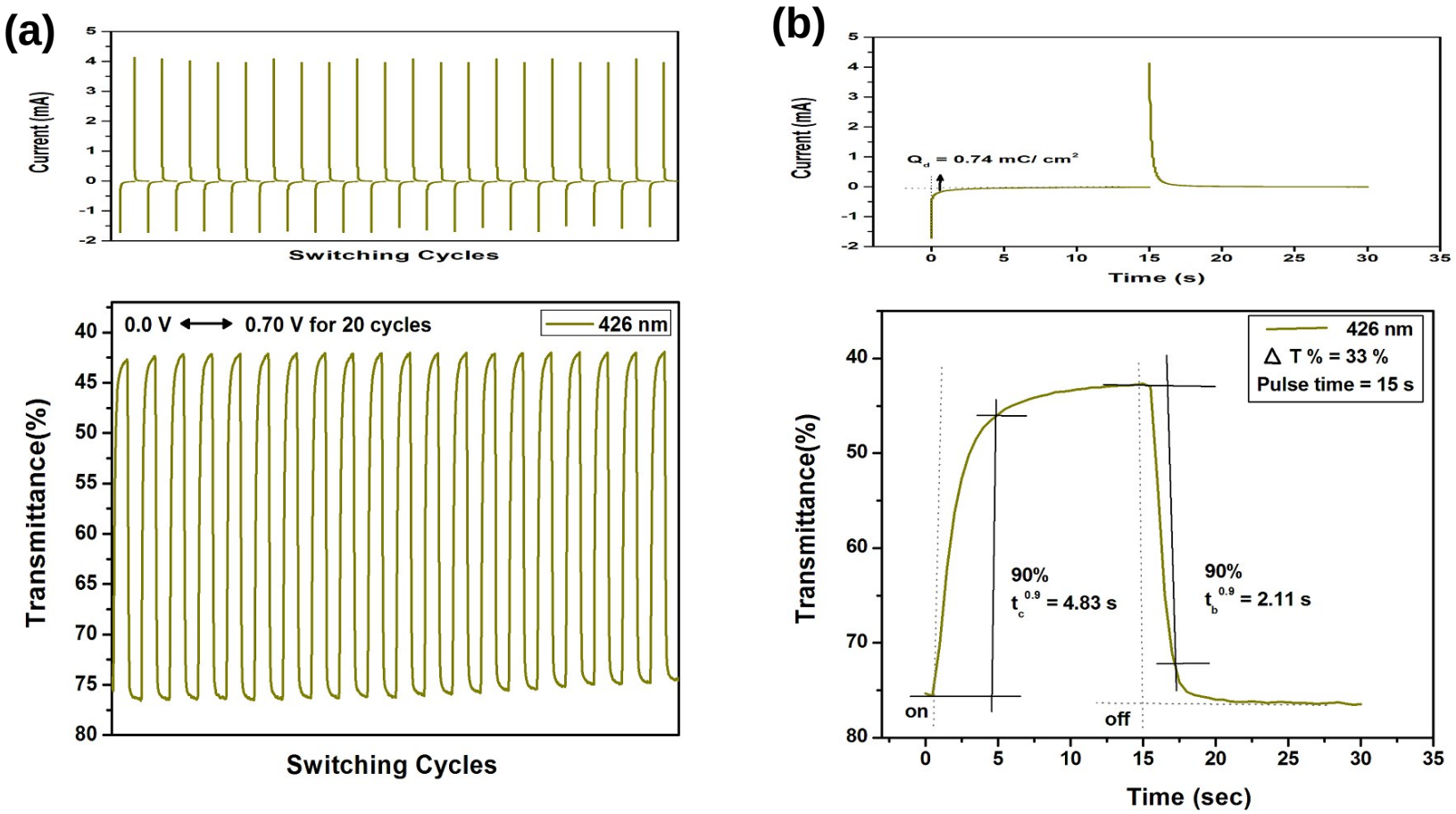

Fig. 11 Potential step absorptiometry of the cast films of **6a** on the ITO-glass slide (coated area ~ 1 cm^2) (in CH_3CN with 0.1 M Bu_4NClO_4 as the supporting electrolyte) by applying a potential step: (a) optical switching at potential 0.00 V ⇔ 0.70 V (20 cycles) and a switching time of 15 s, monitored at λ_{max} = 426 nm; (b) the 1st cycle transmittance change for the **6a** thin film.

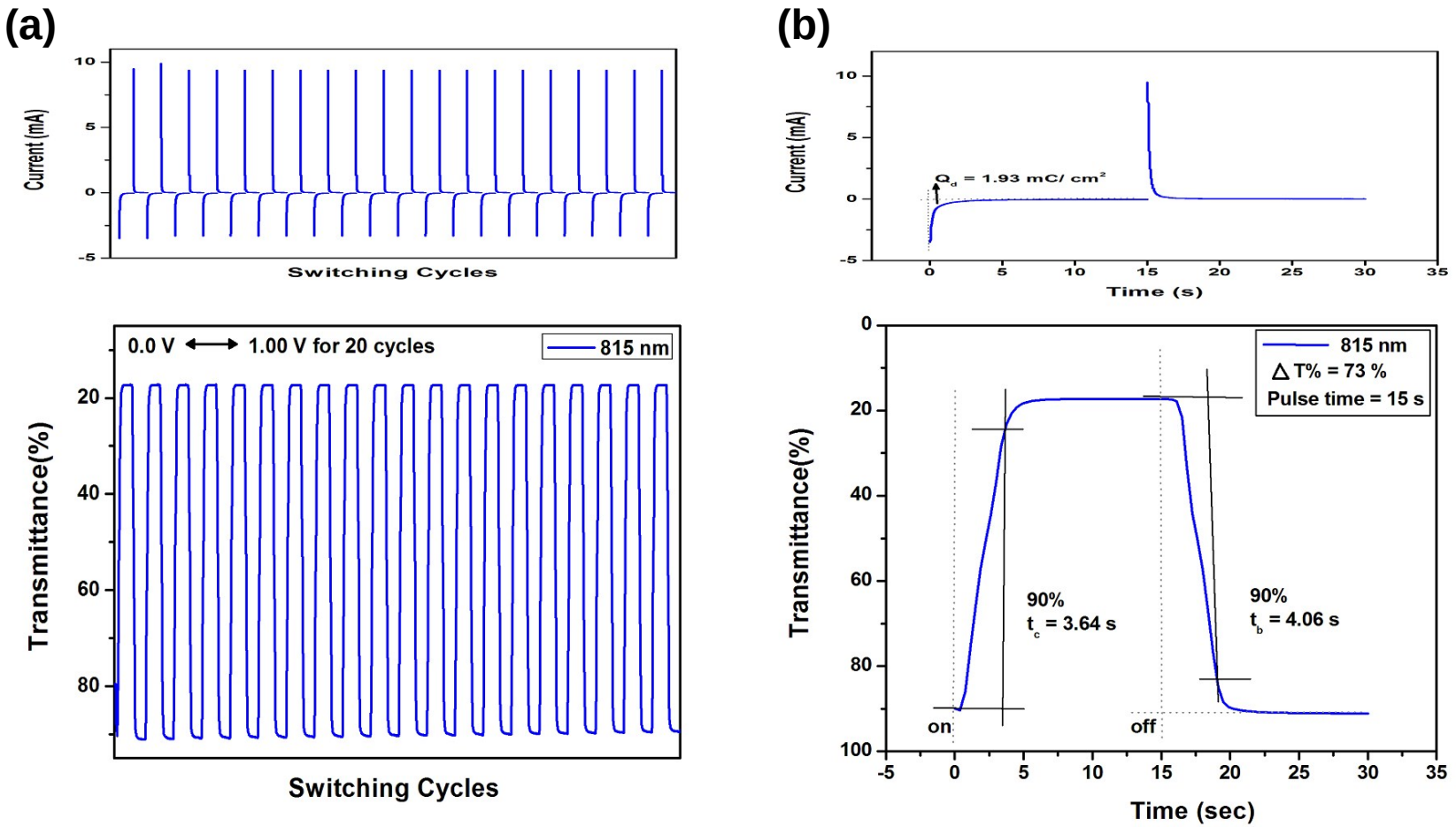

Fig. 12 Potential step absorptiometry of the cast films of **6a** on the ITO-glass slide (coated area ~ 1 cm^2) (in CH_3CN with 0.1 M Bu_4NClO_4 as the supporting electrolyte) by applying a potential step: (a) optical switching at potential 0.00 V ⇔ 1.00 V (20 cycles) and a switching time of 15 s, monitored at λ_{max} = 815 nm; (b) the 1st cycle transmittance change for the **6a** thin film.

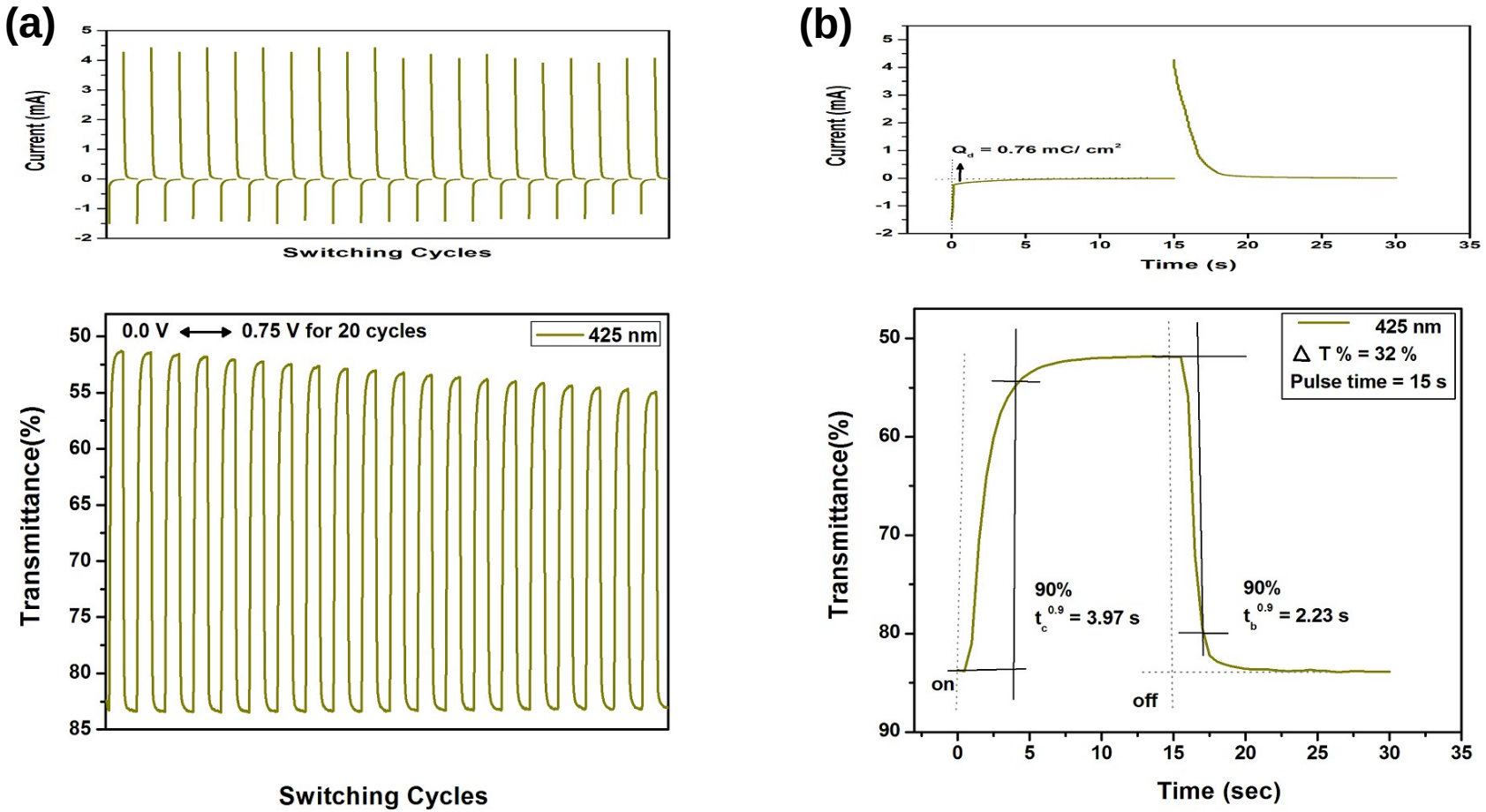

Fig. 13 Potential step absorptiometry of the cast film of **7a** on the ITO-glass slide (coated area ~ 1 cm^2) (in CH_3CN with 0.1 M Bu_4NClO_4 as the supporting electrolyte) by applying a potential step: (a) optical switching at potential 0.00 V ⇔ 0.75 V (20 cycles) and a switching time of 15 s, monitored at λ_{max} = 425 nm; (b) the 1st cycle transmittance change for the **7a** thin film.

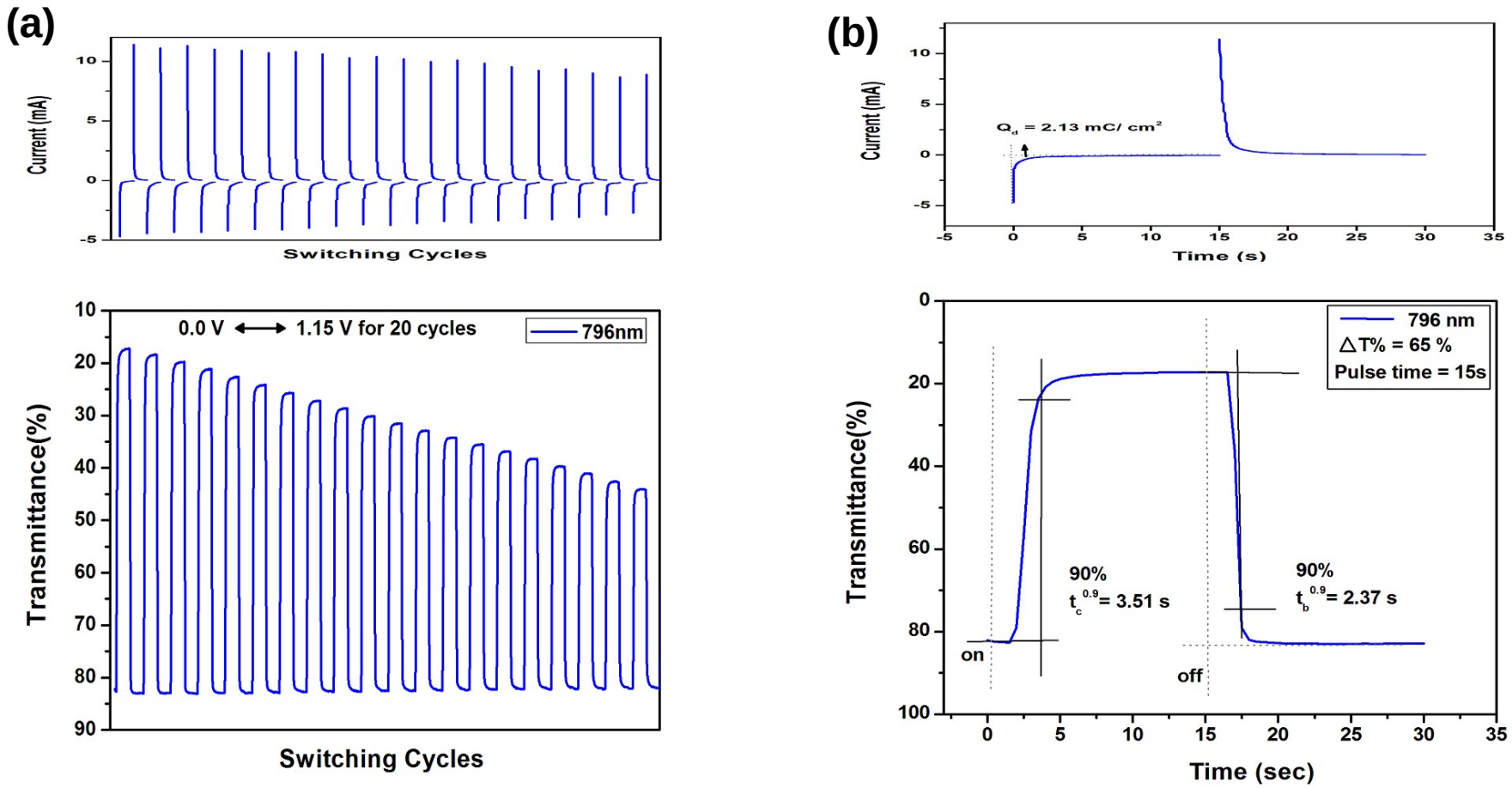

Fig. 14 Potential step absorptiometry of the cast film of **7a** on the ITO-glass slide (coated area ~ 1 cm^2) (in CH_3CN with 0.1 M Bu_4NClO_4 as the supporting electrolyte) by applying a potential step: (a) optical switching at potential 0.00 V ⇔ 1.15 V (20 cycles) and a switching time of 15 s, monitored at λ_{max} = 796 nm; (b) the 1st cycle transmittance change for the **7a** thin film.

Table 4 Electrochromic properties of PAIs

Polymer	λ_{max}[a] (nm)	ΔT%	Response time[b] t_c (s)	Response time[b] t_b (s)	ΔOD[c]	Q_d[d] (mC cm^{-2})	CE[e] (cm^2 C^{-1})
6d	430	36	2.24	1.37	0.232	0.64	362
	817	71	2.70	1.34	0.709	1.76	403
6a	426	33	4.83	2.11	0.235	0.74	318
	815	73	3.64	4.06	0.723	1.93	375
7a	425	32	3.97	2.23	0.216	0.76	284
	796	65	3.51	2.37	0.680	2.13	319
7b	423	31	5.29	3.41	0.214	0.71	301
	812	75	2.19	1.97	0.755	1.95	387

[a] Wavelength of absorption maximum. [b] Time for 90% of the full-transmittance change. [c] Optical density change (ΔOD) = $\log[T_{bleached}/T_{colored}]$, where $T_{colored}$ and $T_{bleached}$ are the maximum transmittance in the oxidized and neutral states, respectively. [d] Q_d is ejected charge, determined from the in situ experiments. [e] Coloration efficiency (CE) =ΔOD/Q_d.

4. Conclusions

A new synthetic procedure for *N,N*'-bis(4-amionophenyl)-*N,N*'-bis(4-methoxyphenyl)-1,4-phenylenediamine was developed. Several novel TPPA(OMe)$_2$-based PAIs have been easily prepared from the imide ring-preformed dicarboxylic acids with the synthesized diamine or from *N,N*'-bis(trimellitimidophenyl)-*N,N*'-bis(4-methoxyphenyl)-1,4-phenylenediamine with aromatic diamines *via* the phosphorylation polyamidation reaction. Because of the presence of TPPA(OMe)$_2$ unit in the main chain, all the polymers exhibited high solubility in many polar aprotic solvents and good film-forming ability. These PAIs also showed moderate to high thermal stability with glass-transition temperatures in the range of 206-292 ^{o}C and 10 wt.-% loss temperatures in excess of 450 ^{o}C. All the PAIs displayed at least two reversible redox waves on their anodic cyclic voltammograms. Incorporating the TPPA(OMe)$_2$ unit on the amide side of PAIs led to lower oxidation potentials, higher redox reversibility, and better electrohromic performance. This new PAI family could be good candidates as anodically electrochromic or hole-transporting materials due to their

proper oxidation potentials, high electrochemical and electrochromic stability, and easy processability.

Acknowledgements

The financial support from the Ministry of Science and Technology, Taiwan, is greatly appreciated.

Notes and references

1 P. M. S. Monk, R. J. Mortimer and D. R. Rosseinsky, *Electrochromism: fundamentals and applications*, VCH, Weinheim, Germany, 1995.

2 P. M. S. Monk, R. J. Mortimer and D. R. Rosseinsky, *Electrochromism and electrochromic devices.* Cambridge University Press, Cambridge, UK, 2007.

3 R. J. Mortimer, *Chem. Soc. Rev*., 1997, **26**, 147–156.

4 D. R. Rosseinsky and R. J. Montimer, *Adv. Mater.*, 2001, **13**, 783–793.

5 (*a*) R. D. Rauch, *Electrochim. Acta*, 1999, **44**, 3165–3176; (*b*) R. Baetens, B. P. Jelle and A. Gustavsen, *Sol. Energy Mater. Sol. Cells*, 2010, **94**, 87–105.

6 http://www.gentex.com and associated pages.

7 A. P. Weidner, U. S. Patent No. 7450294, 2008.

8 G. H. Sonmez and B. Sonmez, *J. Mater. Chem*., 2006, **16**, 2473–2477.

9 R. J. Mortimer, A. L. Dyer and J. R. Reynolds, *Displays*, 2006, **27**, 2-18.

10 S. Beaupre, A.-C. Breton, J. Dumas and M. Leclerc, *Chem. Mater*., 2009, **21**, 1504–1513.

11 G. Sonmez, *Chem. Commun.,* 2005, 5251–5259.

12 A. Patra and M. Bendikov, *J. Mater. Chem.,* 2010, **20**, 422–433.

13 P. M. Beaujuge and J. R. Reynolds, *Chem. Rev.,* 2010, **110**, 268–320.

14 A. Balan, D. Baran and L. Toppare, *Polym. Chem*., 2011, **2**, 1029–1043.

15 G. Gunbas and L. Toppare, *Chem. Commun.,* 2012**, 48**, 1083–1101.

16 P. M. Beaujuge, C. M. Amb and J. R. Reynolds, *Acc. Chem. Res.,* 2010, **43**, 1395–1407.

17 C. M. Amb, P. M. Beaujuge and J. R. Reynolds, *Adv. Mater*., 2010, **22**, 724–728.

18 A. L. Dyer, M. R. Craig, J. E. Babiarz, K. Kiyak and J. R. Reynolds, *Macromolecules,* 2010, **43**, 4460–446.

19 C. M. Amb, A. L. Dyer and J. R. Reynolds, *Chem. Mater.,* 2011, **23**, 397–415.

20 A. L. Dyer, E. J. Thompson and J. R. Reynolds, *ACS Appl. Mater. Interfaces,* 2011, **3**, 1787–1795.

21 M. Thelakkat, *Macromol. Mater. Eng*., 2002, **287**, 442–461.

22 Y. Shirota, *J. Mater. Chem.,* 2005, **15**, 75–93.

23 Y. Shirota and H. Kageyama, *Chem. Rev*., 2007, **107**, 953–1010.

24 S.-H. Cheng, S.-H. Hsiao, T.-H. Su and G.-S. Liou, *Macromolecules,* 2005, **38**, 307–316.

25 C.-W. Chang, G.-S. Liou and S.-H. Hsiao, *J. Mater. Chem.,* 2007, **17**, 1007–1015.

26 S.-H. Hsiao, G.-S. Liou, Y.-C. Kung and H.-J. Yen, *Macromolecules,* 2008, **41**, 2800–2808.

27 Y.-C. Kung and S.-H. Hsiao, *J. Mater. Chem*., 2010, **20**, 5481–5492.

28 H.-M. Wang and S.-H. Hsiao, *Polym. Chem*., 2010, **1**, 1013–1023.

29 Y.-C. Kung and S.-H. Hsiao, *J. Mater. Chem.*, 2011, **21**, 1746–1754.

30 H.-J. Yen and G.-S. Liou, *Polym. Chem.,* 2012, **3**, 255–264.

31 H.-M. Wang and S.-H. Hsiao, *J. Mater. Chem. C*, 2014, **2**, 1553–1564.

32 J.-H. Wu and G.-S. Liou, *Adv. Funct. Mater*., 2014, **24**, 6422–6429.

33 Y. Imai, in *Synthesis of Polyamideimides in Polyimide*: *Fundamentals and Applications*, ed. M. K. Ghosh and K. L. Mittal, Marcel Dekker, New York, 1996, pp. 49–70.

34 N. Yamazaki, M. Matsumoto and F. Higashi, *J. Polym. Sci., Polym. Chem. Ed.,* 1975, **13**, 1373–1380.

35 (*a*) C.-P. Yang and S.-H. Hsiao, *Makromol. Chem.,* 1989, **190**, 2119–2131; (*b*) S.-H. Hsiao and C.-P. Yang, *J. Polym. Sci. A: Polym. Chem.*, 1990, **28**, 1149–1159; (*c*) S.-H. Hsiao and C.-P. Yang, *Makromol. Chem*., 1990, **191**, 155–167.

36 (*a*) D.-J. Liaw, P.-N. Hsu, W.-H. Chen and S.-L. Lin, *Macromolecules,* 2002, **35**, 4669–4676; (*b*) H. Behniafar and A. Banihashemi, *Polym. Int*., 2004, **53**, 2020–2025; (*c*) H.-M. Wang and S.-H. Hsiao, *Polym. Chem*., 2010, **1**, 1013–1023; (*d*) I. Bacosca, E. Hamciuc, M. Bruma and M. Ignat, *React. Funct. Polym*., 2011, **71**, 905–915; (e) S.-H. Hsiao, W. Guo, T.-H. Tsai and Y.-T. Chiu, *J. Polym. Res*., 2014, **21**:391 (10 pages).

37 E. T. Seo, R. F. Nelson, J. M. Fritsch, L. S. Marcoux, D. W. Leedy and R. N. Adams, *J. Am. Chem. Soc.,* 1966, **88**, 3498–3503.

38 S.-H. Hsiao, Y.-M. Chang, H.-W. Chen and G.-S. Liou, *J. Polym. Sci. A: Polym. Chem.,* 2006, **44**, 4579–4592.

39 G.-S. Liou and C.-W. Chang, *Macromolecules,* 2008, **41**, 1667–1674.

40 C.-W. Chang, C.-H. Chung and G.-S. Liou, *Macromolecules,* 2008, **41**, 8441-8451.

41 C.-W. Chang and G.-S. Liou, *J. Mater. Chem.,* 2008, **18**, 5638–5646.

42 H.-M. Wang and S.-H. Hsiao, *Polymer*, 2009, **50**, 1692–1699.

43 S.-H. Hsiao, G.-S. Liou and H.-M. Wang, *J. Polym. Sci. A: Polym. Chem.*, 2009, **47**, 2330–2343.

44 H.-M. Wang and S.-H. Hsiao, *J. Polym. Sci. A: Polym. Chem.*, 2011, **49**, 337–351.

45 H.-J. Yen and G.-S. Liou, *Chem. Mater*., 2009, **21**, 4062–4070.

46 C.-J. Chen, H.-J. Yen, W.-C. Chen and G.-S. Liou, *J. Mater. Chem*., 2012, **22**, 14085–14093.

47 N. P. Buu-Hoi, *J. Chem. Soc*., 1592, 4346.

48 M. B. Robin and P. Day, *Adv. Inorg. Chem. Radiochem*., 1968, **10**, 247–422.

49 C. Lambert and G. Noll, *J. Am. Chem. Soc*., 1999, **121**, 8434–8442.